Journal of Materials Chemistry

Cite this: J. Mater. Chem., 2012, 22, 22272

www.rsc.org/materials

PAPER

A slow relaxing species for molecular spin devices: EPR characterization of static and dynamic magnetic properties of a nitronyl nitroxide radical†

A. Collauto,[a] M. Mannini,[b] L. Sorace,[b] A. Barbon,[ac] M. Brustolon*[ac] and D. Gatteschi*[b]

Received 30th July 2012, Accepted 4th September 2012
DOI: 10.1039/c2jm35076a

Nitronyl nitroxides (NitR) are a family of persistent radicals widely used in molecular magnetism and recently suggested as potential candidates for spintronic applications. In this paper we characterize by X- and W- band Electron Paramagnetic Resonance (EPR) spectroscopy the new radical *S*-4-(nitronyl nitroxide) benzyl ethanethioate (NitSAc) designed for assembling on Au surfaces. We determined the radical magnetic tensors and studied by X-band pulse EPR its spin relaxation behaviour in fluid and glassy solutions of toluene. A comparison with the well known nitroxide 3-carbamoyl-2,2,5,5-tetramethyl-3-pyrrolin-1-oxyl (CTPO) is afforded. The advantages of using NitSAc in technological applications are discussed on the basis of the slow spin relaxation demonstrated by this study.

Introduction

Nitronyl nitroxides (NitR) are well-known stable radicals in which the unpaired electron is essentially delocalized over two equivalent NO groups.[1,2] They have interesting properties, since their ability as bridging ligands towards metal ions makes them suitable as building blocks in designing molecular based magnetic materials,[3,4] and the strong π spin polarization favours a direct ferromagnetic exchange between neighbouring molecules in the solid state. A molecular crystal of a nitronyl nitroxide was the first reported example of a purely organic ferromagnet.[5] These radicals are also widely employed to build families of both single chain magnets and single molecule magnets.[6–11] More recently, their use has been suggested as elementary molecular two level systems to be used in molecular spin based Quantum Information Processing (QIP).[12] Among the main advantages of these systems compared to other potential implementation of Quantum Computers (QC), one has to consider that qubit scalability can be achieved by appropriate synthetic strategy.[13] The use of organic radicals has further been suggested to present some advantages compared to the use of transition metal based clusters,[14–19] as they do not contain metal centers which may represent an intrinsic limitation for qubits encoding due to their single ion anisotropy. More interestingly, organic radicals often show a simple and flexible chemistry, which can be used to promote grafting and organization in nanostructures; this approach makes them addressable using appropriate techniques.[20–22] On the other hand, they suffer from the same limitations, for use in QIP, as any other potential electron spin qubit, namely a stronger coupling with the environment which makes decoherence related issues much more difficult to solve than in *e.g.* photon based QCs.[13] The absolute need for a deep characterization of the relaxation dynamics of these systems in different environments, trying to understand which factors are crucial in determining their spin relaxation behaviour, is then clear. This would then allow identifying the degrees of freedom that affect more the relaxation processes, and on this basis to fine tune the properties of the system by appropriate chemical modification. This approach has been recently undertaken for chromium ring based molecules,[23] among the most relevant candidates for QC applications of molecular magnets.[24,25] It is worth noting that such a deep characterization of the relaxation dynamics of organic radicals may promote the routine use of NitR radicals in more traditional applications, *e.g.* as spin probes or spin labels in advanced Electron Paramagnetic Resonance (EPR) techniques.[26]

Among the vast family of NitR organic radicals we have recently undertaken a full characterization by cw-EPR of *p*-methyl-thio-phenyl-nitronyl nitroxide (MTPNN), both in isotropic[27] and ordered nematic phases,[28] by exploiting an innovative modeling strategy alternative to the usual spectral simulation approach.[29] This study was intended to open the way to the characterization of EPR spectra of Self-Assembled Monolayers (SAMs) of the same radical, in particular under the aspect of the ordering and hindered mobility associated with the bidimensional quasi-regular structure of the monolayer anchored to a solid substrate. In this perspective, the research activity of some of us in the assembling of NitR on surfaces led us to tailor their chemical structure by appropriately selecting the linking group which promotes the selective interaction of the

[a]*Dipartimento di Scienze Chimiche, Università degli Studi di Padova, Via Marzolo, I-35131 Padova, Italy. E-mail: marinarosa.brustolon@unipd.it*
[b]*Dipartimento di Chimica "Ugo Schiff", Università degli Studi di Firenze & INSTM RU Firenze, Via della Lastruccia 3, 50019 Sesto Fiorentino, FI, Italy. E-mail: dante.gatteschi@unifi.it*
[c]*INSTM RU Padova, Via Marzolo, I-35131 Padova, Italy*
† Paper dedicated to the memory of Prof. Giacomo Martini.

molecules with a gold surface. To avoid problems related to the chemical instability of NitR in the presence of free thiols, a methyl-sulphide functionalization was originally chosen. This strategy allowed the optimization of the spacer group between the surface and the radical in order to achieve the highest control of the organization on the surface.[20] However, the use of this linker suffered from the ambiguity about the way alkyl-sulphides anchor on gold, *i.e.* with or without a C–S cleavage.[30–32] To avoid this problem and to improve further the assembling of NitR on gold, a possible solution[33] is the use of a thio-acetyl function as a linker group, by preparing the *S*-4-(nitronyl nitroxide) benzyl ethanethioate radical (hereafter NitSAc).

In this paper we describe a complete characterization of the EPR-related properties of NitSAc with a particular emphasis on its spin relaxation behaviour, both in fluid and glassy solutions of toluene. As previously stated, a thorough characterization of the EPR-related properties of the radical, with a special emphasis on the determination of the magnetic tensors, is required in order to interpret the spectra obtained from SAMs. We wish to show how our multifaceted approach can be a first step to describe the magnetic properties of NitRs, both static (magnetic tensors) and dynamic (relaxation rates), in view of their potential applications either as spin probes/spin labels in EPR spectroscopy or as fundamental units of QC exploiting pulse EPR techniques. We will also characterize in the same experimental conditions a nitroxide radical, CTPO (3-carbamoyl-2,2,5,5-tetramethyl-3-pyrrolin-1-oxyl), to compare, in particular, the relaxation rates of the two radicals; in this respect it is worth noting that – among other nitroxides characterized by similar size and magnetic tensors – CTPO is characterized by a quite rigid structure, and it is expected to have rather slow relaxation rates as the impact of internal motions on the electron spin relaxation should be small.

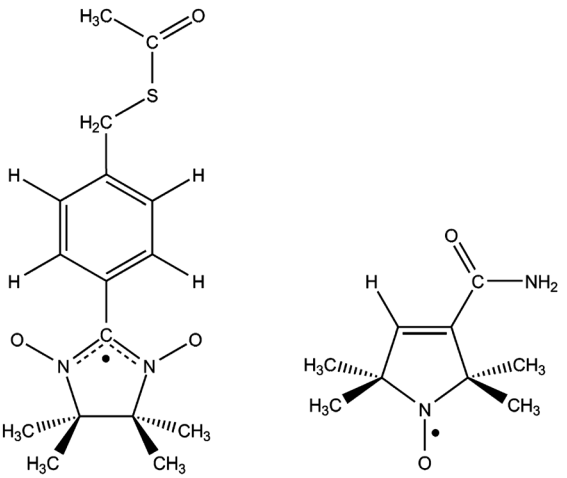

Scheme 1 Structural formulae of the radicals *S*-4-(nitronyl nitroxide) benzyl ethanethioate (NitSAc) and 3-carbamoyl-2,2,5,5-tetramethyl-3-pyrrolin-1-oxyl (CTPO).

Experimental

All starting materials were purchased from Aldrich. High purity solvents were used without additional purification steps. The radical was obtained by following the procedure previously reported by Gorini,[34] which we briefly summarize in the following: NitSAc (Scheme 1) was synthesized starting from the coupling of *S*-4-acetylbenzyl ethanethioate with 2,3-di(hydroxyamino)-2,3-dimethylbutane exploiting a TPAP-NMO based strategy to avoid overoxidation problems.[35] The obtained product, purified by flash column chromatography, yielded a blue microcrystalline powder of NitSAc (yield 56%). Anal. calc. for $C_{16}H_{21}N_2O_3S$ C 59.78, H 6.58, N 8.72. Found: C 61.12, H 6.07, N 9.52%. IR (KBr, cm^{-1}): 2964–2852 (ν_{C-H}, m), 1688 ($\nu_{C=O}$, s), 1366 (ν_{N-O}, s), 1132–1100 (ν_{S-C}, m), 802 ($\nu_{C-H}^{bending}$, m).[33]

The radical was then dissolved in anhydrous toluene to a concentration of 50 μM and put into a 2 mm (i.d.) quartz tube. The samples were carefully deaerated by 3–4 freeze–pump–thaw cycles, and then sealed under vacuum. The same procedure was used to prepare a sample of the CTPO (Aldrich) nitroxide spin label (Scheme 1). The absence of other radicals was verified by EPR.

Continuous wave (CW) and pulse X-band EPR experiments were performed using a Bruker Elexsys E580 spectrometer equipped with a Bruker ER4118X-MD5 dielectric ring resonator inside a cryostat (CF935 Oxford Instruments) cooled by nitrogen flow for variable temperature operation. CW-EPR spectra in the fluid phase were recorded at a microwave power of about 20 μW; the modulation frequency was set to 100 kHz with an amplitude of 0.1 G. Higher resolution spectra were recorded setting the modulation frequency to 3.5 kHz with an amplitude of 25 mG; these parameters allowed us to avoid spectral line shape distortion at the expense of the signal-to-noise ratio. In frozen solution, much broader linewidths allowed us to use a modulation amplitude of 1 G.

In pulse EPR experiments the primary echo was generated with a standard $\pi/2$–τ–π–τ–echo sequence; the two-pulse echo decay (or Hahn decay) traces were recorded by monitoring the top of the echo on varying the delay τ between the pulses, whereas the echo-detected EPR (ED-EPR) spectra were obtained by integrating the whole primary echo while sweeping the magnetic field for a fixed delay between the pulses. For this last experiment soft pulses ($\pi/2$ = 48 ns) were used to improve resolution, whereas for the echo decay experiment soft and hard pulses ($\pi/2$ = 8 ns) were used in frozen solution and in fluid solution, respectively (see Results).

The inversion recovery experiments were performed with the usual π–T–$\pi/2$–τ–π–τ-echo scheme upon varying the delay T; the time traces were obtained by integrating the whole echo in the fluid phase or monitoring just the top in frozen solution. In the detection echo sequence the pulses were the same as in the Hahn decay. π-pulses were obtained by doubling the duration of the $\pi/2$ pulse.

The CW-ENDOR experiments were performed in solution with a higher concentration of 370 μM using a Bruker ER200D-SRC X-band EPR spectrometer equipped with a Bruker EN801 ENDOR resonator in a homemade set-up for the radio frequency (RF) control.[28] The spectrum was recorded at 270 K by monitoring the central line of the cw-EPR spectrum; the microwave power was set to 10 mW and the RF modulation frequency was 12.5 kHz with an amplitude of 25 kHz.

W-band EPR spectra were recorded using a Bruker E600 spectrometer equipped with a 6 T split coil magnet (Oxford Instruments) and a continuous flow He cryostat to work at low temperatures. The microwave power was set to 50 dB (50 nW) to exclude saturation effects, which were checked for by measuring spectra at higher power up to 30 dB (5 μW), where saturation starts to set in.

The starting magnetic parameters for the fitting of the experimental spectra were obtained by DFT calculations. The principal values and the principal directions of the Zeeman tensor and of the hyperfine coupling tensors for the two nitrogen nuclei were obtained by QM/DFT calculations with the G09 package[36] using the PBE0 hybrid density functional and the 6-31+G(d,p) basis set. Solvent effects on both the minimum energy conformation and the magnetic tensors were taken into account using the implementation of the polarizable continuum model (PCM[37]) provided by G09. In the fitting procedure we considered the hyperfine structure due to the protons as giving an inhomogeneous broadening of the ^{14}N hyperfine components; the corresponding inhomogeneous linewidth was allowed to be orientation dependent, to take into account the appreciable anisotropy of the hyperfine splitting of the two phenyl *ortho* protons, which shows a maximum along the y principal axis of the $\boldsymbol{g}$ tensor.[28]

Results

Spectral properties

Fluid solution. CW-EPR spectra (Fig. 1) of the diluted (50 μM) solution of NitSAc in toluene were obtained at various temperatures in the interval 180–300 K. They show the typical 1 : 2 : 3 : 2 : 1 intensity pattern arising from the coupling of the unpaired electron with two equivalent ^{14}N ($I = 1$) nuclei. In the following we will refer to these hyperfine components by their total nuclear spin quantum numbers $M_I = m_{I1} + m_{I2}$. Each of the five M_I lines is further split into a number of components due to hyperfine interaction with protons (Fig. 2). This hyperfine structure consists of a complex pattern whose resolution, dependent on linewidth, varies with the temperature and with the ^{14}N hyperfine component. We have analyzed the central line ($M_I = 0$) for $T = 270$ K, showing the best resolution of the proton splitting. A best fit simulation (see Fig. 2) gives three coupling constants: 0.47 G (2 equivalent protons), 0.28 G (2 equivalent protons) and 0.21 G (12 equivalent protons). The three hyperfine coupling constants (hfccs) are attributed respectively to the two pairs of phenyl protons in *ortho* and *meta* positions with respect to the nitronyl nitroxide residue, and to the twelve equivalent methyl protons.[38] These assignments are confirmed by the analysis of the CW-ENDOR spectrum, shown in Fig. 3: simulation of the spectrum allowed us to extract two proton hfccs with constants of 1.31 MHz (0.47 G) and 0.58 MHz (0.21 G). The two lines relative to two protons with hfcc of 0.28 G are not detectable as they are completely covered by the pair of strong lines relative to the twelve methyl protons. The two lines observed at the lower frequency, due to ^{14}N nuclei, are centered at $a_N/2$, and separated by twice the free ^{14}N nuclear Larmor frequency ν_N. The value of a_N (7.45 G) is in agreement with the value obtained from the nitrogen nuclei hyperfine pattern in Fig. 1 and 4, see below.

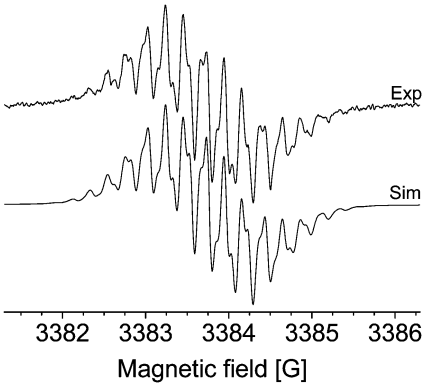

Fig. 2 CW-EPR spectrum of a 50 μM solution of NitSAc in toluene at 270 K recorded for the $M_I = 0$ hyperfine component under high resolution conditions.

We obtained very intense ED-EPR spectra in fluid solution in the range 180–300 K by using soft pulses ($\pi/2 = 48$ ns) and with an inter-pulse delay of 500 ns, see Fig. 4.

The five lines, separated by a_N, do not show the proton hyperfine structure as the experimental conditions were not selective enough. The intensities of the lines are weighted by the different decays of the electron spin echo, which are dependent

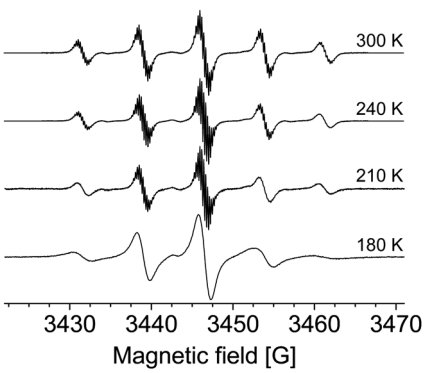

Fig. 1 CW-EPR spectra of a 50 μM solution of NitSAc in toluene recorded in the fluid phase.

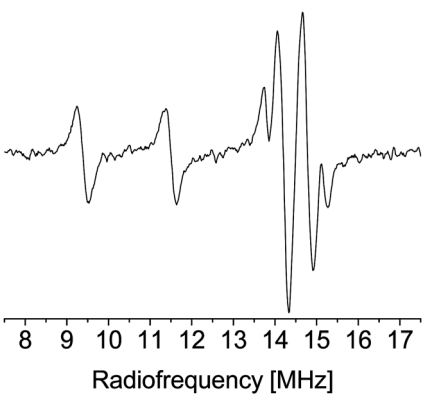

Fig. 3 CW-ENDOR spectrum of a 370 μM solution of NitSAc in toluene recorded at 270 K; the two lines at lower frequency are attributed to the ^{14}N ENDOR transitions.

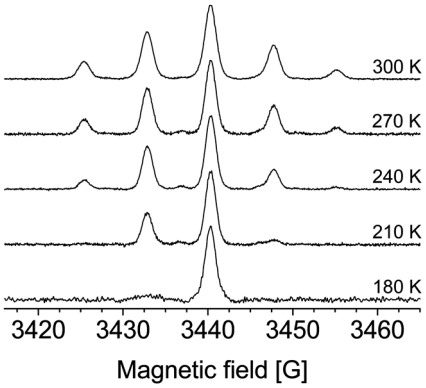

Fig. 4 ED-EPR spectra of a 50 μM solution of NitSAc in toluene recorded in the fluid phase with $\tau = 500$ ns.

on the nuclear spin configuration (m_{I1},m_{I2}) of the two ^{14}N nuclei contributing to M_I. This will be discussed further below.

Glassy matrix. CW-EPR spectra at X-band (Fig. 5) were recorded in the range 80–150 K. The spectrum does not show appreciable changes up to 120 K; for higher temperatures, slight alterations of the spectral profile indicate a residual mobility of the radical.

To improve the reliability of the results obtained by simulation, a rigid limit spectrum (100 K) at W-band was also recorded (Fig. 6), showing a clear resolution of the ***g***-tensor anisotropy.

Spectra at both frequencies were simulated by the EasySpin software package.[39] A global best fit procedure was performed by a simultaneous fit of the spectra at both frequencies; the fit required a refining of the principal values and the principal directions of the Zeeman tensor and of the hyperfine coupling tensors for the two nitrogen nuclei taking the starting values from the output of a QM/DFT calculation (see Experimental); in the refinement process the principal values of the hyperfine tensors were kept equal. The QM calculation shows that a tilt angle φ between the z principal axes of the nitrogen hyperfine tensors and the ***g***-tensor is present. Refinement of the tensors to fit the experimental spectra shows, furthermore, that the z principal directions of the two nitrogen tensors are not symmetrically

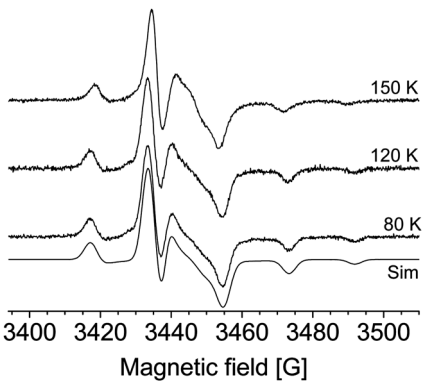

Fig. 5 CW-EPR spectra of a 50 μM solution of NitSAc in toluene recorded in the glassy matrix. For the 80 K spectrum the power was reduced to 2 μW to avoid microwave power saturation.

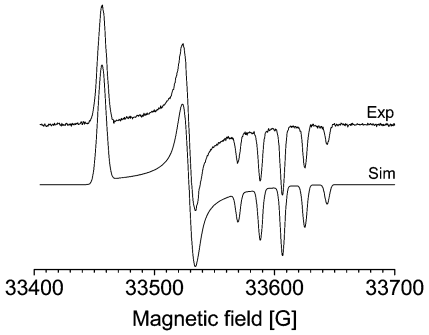

Fig. 6 CW-EPR spectrum of a 50 μM solution of NitSAc in toluene recorded at W-band in the glassy matrix.

tilted with respect to the ***g***-frame (see Table 1); the relative tilt angle obtained between the two z principal directions of the nitrogens is slightly larger than 9°.

The same magnetic parameters resulting from the global fit also led to a satisfactory reproduction of the ED-EPR spectra shown in Fig. 7. These latter spectra were recorded in order to get information on the dependence of the phase memory time T_M on the resonance magnetic field and, therefore, on the residual mobility of the paramagnetic probe[40] also at temperatures giving rigid limit CW-EPR spectra. ED-EPR spectra show effects on the spectral profile upon varying the inter-pulse delay τ down to 80 K. This observation is in agreement with the ED-EPR studies on nitroxides in glassy solids,[40] where the orientation dependent relaxation has been attributed to low-amplitude fast librational motions of the probe in the matrix. We used a simple model for such a motion, considering it as a jump of the radical between two orientations that are produced by a rotation around an axis d.[41] Under the fast motion condition the relaxation rate due to the librational motion is given as[41]

$$\frac{1}{T_M(m_{I1}, m_{I2}, \Omega, \Phi)} = \tau_L[\Delta\omega(m_{I1}, m_{I2}, \Omega, \Phi)]^2 \qquad (1)$$

where Ω is the set of Euler angles defining the director of the magnetic field in the molecular frame, Φ is the librational angle specifying the displacement of the director of the magnetic field, $\Delta\omega(m_{I1},m_{I2},\Omega,\Phi)$ is the difference between the resonance frequencies corresponding to the two orientations for a given nuclear spin configuration (m_{I1},m_{I2}), and τ_L is the correlation time for the exchange process.

Table 1 Principal values of ***g***, nitrogen hyperfine ($\boldsymbol{A}_N$) magnetic tensors and ^{14}N isotropic hfccs. The tilt angle φ between the z principal directions of the $\boldsymbol{A}_N$ and that of the ***g*** tensors is reported

Magnetic tensor/unit	Principal values	φ
g	2.0111_1, 2.0067_1, 2.0021_1	—
$\langle g\rangle = 1/3Tr\{\boldsymbol{g}\}$	2.0066_3	
$\boldsymbol{A}_{N1}$/G	0.0_1, 1.6_1, 18.6_1	$7.7_5°$
$\langle A_{N1}\rangle = 1/3Tr\{\boldsymbol{A}_{N1}\}$/G	6.7_3	
$a_{0,N1}$ (fluid solution)/G	7.45_5	
$\boldsymbol{A}_{N2}$/G	0.0_1, 1.6_1, 18.6_1	$1.6_5°$
$\langle A_{N2}\rangle = 1/3Tr\{\boldsymbol{A}_{N2}\}$/G	6.7_3	
$a_{0,N2}$ (fluid solution)/G	7.45_5	

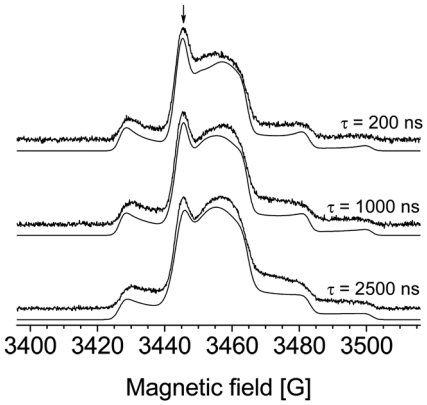

Fig. 7 ED-EPR spectra of a 50 μM solution of NitSAc in toluene recorded at 80 K. Soft pulses ($\pi/2 = 48$ ns) were used with $\tau = 200$ ns (uppermost trace), $\tau = 1000$ ns and $\tau = 2500$ ns (lowermost trace). The arrow denotes the magnetic field position where relaxation measurements were performed.

The best fit between experimental and calculated spectra (Fig. 7) was obtained leaving as free parameters the orientation of the axis d and the amplitude α of the rotation angle, on the basis of typical correlation times τ_L for low-amplitude librational motions.[42] The calculations were performed using a home-written software, which evaluates the resonance field shift due to the libration making use of second-order perturbation theory.[41,43] The best fitting between calculated and experimental profiles was found for an orientation of the axis d tilted by 24° from the z towards the y axis of the $\boldsymbol{g}$ tensor eigenframe (see Fig. 8) and $\alpha = 2.5°$ assuming $\tau_L = 30$ ps.[42]

Relaxation properties

In the following we present the results of the relaxation properties of NitSAc and of the nitroxide radical CTPO for comparison.

Fluid solution. The transverse spin relaxation time T_2 at 292 K was measured by Hahn echo decay ($\pi/2 = 48$ ns) in a series of fluid solutions of NitSAc at decreasing concentrations in order to separate the contribution from the inter-radical Heisenberg exchange. The relaxation rates show a linear dependence on the concentration of the radical with non-zero intercept; the reciprocals of the intercepts of the fitting lines give the T_2^0 values (T_2 values at null concentration). The five T_2^0 values are different, ranging from 0.5 to 1.1 μs at 292 K (see Table 2). We see that the components with $M_I = +1$ and $M_I = 0$ have similar relaxation times, whereas the decay of the $M_I = -1$ component is faster and similar to that of $M_I = +2$ component (lower field line); the $M_I = -2$ component (higher field line) has the shortest T_2^0.

From the slope of the central line we obtain a value for the exchange rate constant $k_{HE} = (3.00 \pm 0.03) \times 10^9\ M^{-1}\ s^{-1} \approx 200\ mG_{pp}\ mM^{-1}$, which is quite similar to the one reported in the literature for perdeuterated Tempone in toluene-d_8 (ref. 44) ($k_{HE} = (3.20 \pm 0.03) \times 10^9\ M^{-1}\ s^{-1} \approx 210\ mG_{pp}\ mM^{-1}$, extrapolated from graph). On the basis of these results we can conclude that at the concentration of 50 μM the exchange contribution is negligible. We measured therefore T_1 and T_2 (or T_M) for NitSAc, the former by echo-detected inversion recovery and the latter by Hahn decay, in fluid and in glassy toluene phases, in the range 180–300 K and 80–120 K respectively. In the temperature range 120–180 K it was impossible to detect the primary echo because of the phase memory time being too short.

The relaxation measurements were also performed for CTPO in the same solvent and concentration at 300, 180, 100 and 80 K to compare the values of the relaxation times for the two radicals.

In fluid solutions T_1 and T_2 were measured for both NitSAc and CTPO with the magnetic field at the central lines of their EPR spectra. The inversion recovery traces were all fitted with a monoexponential decay function. The echo decay was best fit as

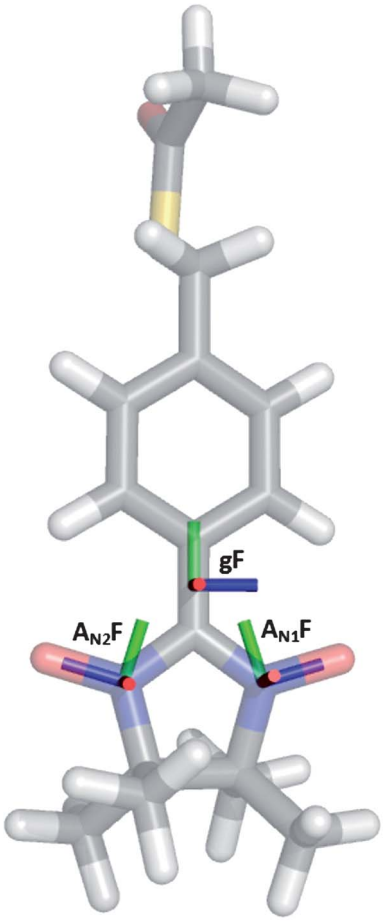

Fig. 8 Magnetic tensor eigenframes (blue: x axis; green: y axis; red: z axis); based upon the local symmetry, the x axes of the nearly axial nitrogen hyperfine coupling tensors have been oriented parallel to the N–O bonds.

Table 2 Linear extrapolation to null concentration (T_2^0) of the T_2 values obtained as a function of the concentration for the five M_I components of NitSAc in toluene at $T = 292$ K

M_I	T_2^0 [μs]
+2	0.79_5
+1	1.04_5
0	1.12_5
−1	0.77_5
−2	0.50_5

a monoexponential in the range 240–300 K and as a biexponential in the range 180–210 K (see Table 3).

As we measured T_2 on the central line with hard pulses (corresponding to a spectral range with a half amplitude value of about ±30 MHz (ref. 45)) we expect contributions from the neighbouring lines with $M_I = +1$ and -1. In the fluid phase at low temperatures we find indeed a biexponential decay of the echo, merging to a monoexponential one at $T = 240$ K as expected when the spin rotational contribution dominates the relaxation for all the hyperfine components (see Discussion). An estimate of the decay times for the neighbouring components can be obtained by the analysis of the relative intensities of the corresponding lines in the ED-EPR spectra (Fig. 4). The fast relaxing components of the biexponential fittings (see Table 3) are consistent with this estimate, hence we attribute the component of the biexponential decay with the longest time and the largest weight to T_2 relative to $M_I = 0$.

In Fig. 9 we report the temperature dependence of T_1 and T_2 in fluid solution for NitSAc (only the longest relaxation time in the range 180–210 K), and the corresponding values at 180 and 300 K for CTPO (at this temperature $T_1 = T_2$).

For NitSAc, T_1 increases monotonically upon decreasing the temperature, whereas T_2 passes through a maximum at around 240 K and drops to very low values as the temperature gets close to the melting point of toluene (178 K (ref. 46)).

Glassy matrix. In the glassy phase T_1 and T_M were measured by the same procedures for NitSAc in the range 80–120 K and for CTPO at 80 K and 100 K. In this phase we checked that the contribution from instantaneous diffusion to the echo dephasing[47] was negligible. We used generally longer pulses ($\pi/2 =$ 48 ns) than in fluid solutions to suppress the echo modulation due to the interaction with nuclei (ESEEM). Both the inversion and the Hahn decay time traces were best fit with biexponential functions.

The magnetic field was set at the position giving the largest echo intensity for CTPO, whereas for NitSAc its value was chosen as shown by the arrow in Fig. 7, on the basis of the following considerations. The powder ED-EPR spectrum of NitSAc is a superposition of the powder spectra obtained for all the nine nuclear spin configurations (m_{I1},m_{I2}), the degeneracy in fluid solution being lost in the glassy matrix as the principal axes of the

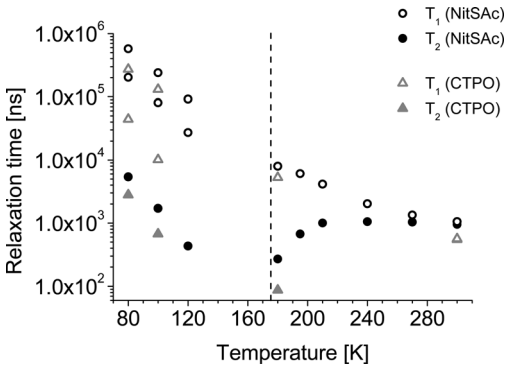

Fig. 9 T_1 and T_2 (T_M) spin relaxation times; the dashed line separates the measurements in the fluid solution (right) from that in the glassy phase (left). In fluid solution the measurements were performed on the central ($M_I = 0$) component of the EPR spectrum both for NitSAc and for CTPO; in the glassy phase the magnetic field was set to the position shown in Fig. 7 for NitSAc and to the position with the largest echo intensity for CTPO.

hyperfine tensors of the two ^{14}N nuclei have different orientations (see above). Therefore at each field one sees a superposition of many echoes characterized, in general, by different relaxation times (see eqn (1)). In order to disentangle the relaxation behaviours we should be able to excite a single type of transition. The deconvolution of the cw-EPR powder spectrum (see Fig. 10) shows that single transitions can be excited by selective pulses only at its wings; however, the echo corresponding to these positions is expected to be very weak. In order to gain intensity we set the field position as shown by the arrow in Fig. 7. For this field, in our experimental conditions ($\pi = 96$ ns) we excite the (+1,0) and the (0,+1) transitions for all the radicals in any orientation. The distributions of resonance fields for these two transitions are the narrowest ones (approximately 6 G wide), giving a quite large signal intensity. The Hahn decay shows a biexponential behaviour with a slow component which is largely dominant. In Fig. 9 we report this latter component as T_M in the glassy phase.

We measured T_1 at the same resonance field as T_M. We also observed in this case a biexponential behaviour; the two components, reported in Fig. 9, have similar weights. We attribute the fast component to spectral diffusion and the slow one to spin lattice relaxation.[48] In the same graph we also show the

Table 3 Relaxation times as obtained from inversion recovery (T_1) and two pulse echo decay (T_2) experiments for NitSAc and CTPO in toluene solution. In parentheses the weight of the relative component in biexponential fits is reported

NitSAc					CTPO			
T [K]	$T_{1,A}$ [μs]	$T_{1,B}$ [μs]	$T_{2,A}$ [μs]	$T_{2,B}$ [μs]	$T_{1,A}$ [μs]	$T_{1,B}$ [μs]	$T_{2,A}$ [μs]	$T_{2,B}$ [μs]
300	1.05_1		0.95_1		0.56_1		0.550_5	
270	1.34_1		1.035_5					
240	2.03_1		1.055_5					
210	4.14_1		1.00_2 (50%)	0.40_1				
195	6.08_1		0.67_2 (60%)	0.26_1				
180	7.95_4		0.27_1 (70%)	0.11_2	5.3_4		0.09_1	
120	92_1	27_1	0.43_1					
100	240_5	81_3	1.7_2 (35%)	0.6_1	131_6 (60%)	10_1	0.67_2	
80	580_{10}	203_4	5.41_5[a]		275_5 (55%)	44_2	2.79_4 (85%)	0.12_3

[a] Obtained by fitting with a stretched exponential[54] with $x = 3/2$.

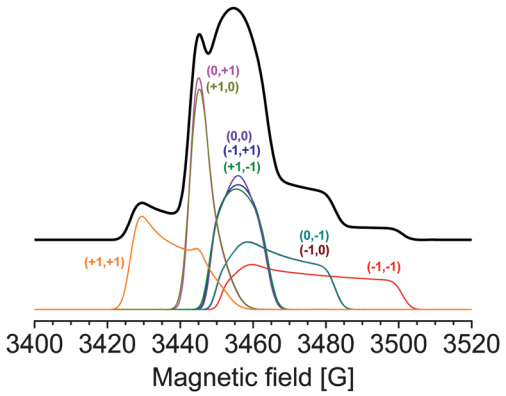

Fig. 10 Sum (black thick line) and deconvoluted (coloured lines) powder CW-EPR spectrum of NitSAc in frozen toluene (T = 80 K); the components are indexed according to their (m_{I1},m_{I2}) values (see text).

corresponding values for CTPO at $T = 80$ K and 100 K, both of which are shorter than the corresponding values for NitSAc (at 80 K respectively, 577 and 207 μs for the latter and 270 and 44 μs for CTPO).

Discussion

Let us discuss separately the results of the magnetic tensors of NitSAc and of the relaxation properties of NitSAc and CTPO.

Magnetic tensors

Information as accurate as possible on the principal values of the magnetic tensors and on the mutual orientation between their principal axes is of fundamental importance when using the radical as a spin probe in advanced EPR applications[26,49] and for implementation in QIP.[50] For these reasons, we used a hybrid theoretical/experimental approach for their determination,[27–29] which consists, as explained in the Results section, of the calculation of the principal axes and principal values of the $\boldsymbol{g}$ and hyperfine tensors by QM/DFT methods and their refinement *via* best fitting of the experimental spectra in the glassy phase. The reliability of the results lies on the fact that (a) the principal values have been obtained from the best fit of the X-band and the W-band spectra together (see Fig. 5 and 6, Table 1) (b) the obtained principal values compare well with those reported in the literature for similar radicals[27,51–53] (c) the principal directions and values of the ^{14}N hyperfine tensors obtained by this global fit have been also used to simulate the ED-EPR spectra, which are extremely sensitive to small changes in the z principal directions of the hyperfine coupling tensors. This is a relevant result, since – to the best of our knowledge – this is the first time that the nitrogen nuclei hyperfine coupling tensors and the mutual orientation of the magnetic tensors of a NitR radical have been both experimentally determined.

For a spin distribution on a planar ONCNO fragment with a C_2 symmetry axis one would expect that the z axes of the ^{14}N hyperfine tensors should be symmetric with respect to the symmetry axis. However, as reported in Fig. 8 and in Table 1, the two ^{14}N hyperfine coupling tensors do not follow this expected symmetry, indicating that at low temperatures the technique is sensitive enough to monitor a small distortion from C_2 symmetry. On the other hand at high temperatures the conformation shows the twofold symmetry, as proved by the identical isotropic hfccs. We conclude that in fluid solution there is a fast intramolecular motion between two equivalent non-planar conformations, giving rise to a symmetric average conformation of the fragment. On lowering the temperature the interconversion rate decreases, eventually leading to two equivalent but asymmetric conformations. A similar type of interconversion between two equivalent twisted-crossover conformations, becoming "fast" for $T > 230$ K, has been previously reported for the nitroxide radical Tempone in a solid host matrix.[54]

Finally, we note that the proton experimental hfccs in fluid solution, obtained by the simulation of the central EPR line at 270 K and further checked by ENDOR, are consistent with proton hfccs reported in the literature for similar molecules,[38,55,56] apart from the *ortho* phenyl protons. We attribute this latter difference to the effect induced by the CH_2–S–R residue in the *para* position with respect to the nitronyl nitroxide ring.

Relaxation properties

Fluid solution. In fluid solution the transverse relaxation times at zero concentration, T_2^0, of NitSAc are different for the five lines, as reported above (see Table 2). This is nicely and directly shown by the spectral profile of the ED-EPR spectrum of the diluted fluid solution of the radical reported in Fig. 4. This is in agreement with the expected effect of the time modulation of the magnetic interactions on the relaxation rates of the different ^{14}N hyperfine components, in analogy with the usual results on organic radicals.[57] However, the usual simple Redfield analysis of the $1/T_2$ dependence on the nuclear quantum number M_I, customary for nitroxide radicals, is not suitable in this case due to the presence of degenerate spin states; in order to get relaxation parameters which are comparable with the experimental ones, one should obtain the whole relaxation matrix and diagonalize it.[58] Furthermore, the effect of anisotropic rotational diffusion should be taken into account.[27,59]

A comparison with the results obtained at 300 K for T_1 and T_2 on the central ($M_I = 0$) line of CTPO shows that NitSAc has relaxation times longer by a factor two with respect to the nitroxide (see Fig. 9 and Table 3). At 180 K the ratio between the relaxation times of NitSAc and CTPO is 3 and 1.5 for T_2 and T_1, respectively.

As the relevant contribution to spin relaxation for both radicals comes from the reorientational motion of the molecule,[60] a meaningful comparison between the relaxation times of the two radicals should take into account the different dimensions of the molecules. Let us discuss in the following this issue.

The reorientational motion of a spherical molecule undergoing Brownian rotational diffusion is described by means of the rotational correlation time, which is given by[61]

$$\tau_c = V\frac{\eta}{k_B T} \quad (2)$$

where η is the dynamic viscosity and V is the molecular volume. Equivalent expressions can be defined also for molecules with non-spherical shapes;[62] the main point is that the dependence on the dimensions of the molecule, the temperature and the viscosity is retained.

Among the various contributions to electron spin relaxation, the spin-rotational interaction – arising from the coupling between the angular momentum of the tumbling molecule and the spin[63] – gives equal terms to both the transverse and the longitudinal relaxation rates:[64]

$$\frac{1}{T_1^{SR}} = \frac{1}{T_2^{SR}} = \frac{1}{9}\frac{(\Delta g : \Delta g)}{\tau_c} \quad (3)$$

where $(\Delta g{:}\Delta g) = (g_{xx} - g_e)^2 + (g_{yy} - g_e)^2 + (g_{zz} - g_e)^2$ and g_e is the free electron g value. At high temperatures the contribution to T_1 and T_2 from spin-rotation has been shown to become dominant, hence making $T_1 = T_2$,[60] as in the present case. This consideration allows us to estimate the ratio between the hydrodynamic volumes of the two radicals in toluene. The values of $(\Delta g{:}\Delta g)$ are 9.54×10^{-5} for NitSAc (see Table 1) and 5.85×10^{-5} for CTPO.[65] From eqn (2) and (3) we get V(NitSAc)/V(CTPO) $\approx$ 3. This ratio compares well with the one derived from hydrodynamic modeling of the rotational diffusion tensor;[66] in this case we find V(NitSAc)/V(CTPO) = 2.4.

At lower temperatures in fluid solution the spin-rotational contribution is negligible and the transverse spin relaxation rate is dominated by the secular and pseudosecular contributions;[60] these are proportional to τ_c,[57] a smaller τ_c producing a slower relaxation. However we find that NitSAc has a longer T_2 by a factor of around 3 with respect to the smaller CTPO. We reasonably attribute this behaviour to the different magnitudes of the dipolar hyperfine coupling tensors, which affects the secular and pseudosecular spin relaxation rates.[60]

In summary, at high temperatures, where the spin rotational term dominates the spin relaxation, nitroxides with similar dimensions can in general be competitive with NitSAc, due to their smaller $\boldsymbol{g}$ anisotropy; at lower temperatures, where secular and pseudosecular terms dominate, nitroxides are relaxing much faster than NitSAc, reasonably due to their larger $\boldsymbol{A}$ anisotropy.

Here we note that for NitSAc the opposite dependence on τ_c of the dominant contribution to transverse spin relaxation is responsible for the maximum in T_2 observed at 240 K.

Glassy matrix. For paramagnetic probes in solid matrices the spectral diffusion is competitive with spin lattice relaxation in the recovery of inverted magnetization due to the inescapable selectivity of the microwave pulses burning a hole in the spectrum. The disentanglement of the two characteristic times has been studied in detail and various methods have been proposed for the scope.[48,67,68] In the present case our main scope was a comparison between the relaxation behaviours of the radicals NitSAc and CTPO, therefore in the glassy matrix we limited ourselves to measure the inversion recovery time traces for the two radicals in the same conditions. All the recoveries are given by biexponential functions, and we attribute for all of them the long time to the electronic T_1 of the inverted spin packet, and the short time constant to spectral diffusion to other spin packets. T_1 for CTPO is about one half that of NitSAc (270 μs *vs.* 580 μs), while the spectral diffusion time is, in relative terms, much shorter (45 μs *vs.* 200 μs).

In the temperature range explored in this work for relaxation studies in frozen solution (80–120 K) we have evidence that the relaxation processes are also due to residual motions of the molecule, as discussed below. This is in line with the results on nitroxides in glasses,[69,70] showing a contribution to relaxation due to fast librations. In particular, for $T > 80$ K the Hahn decay shows an exponential behaviour typical of a dominant relaxation due to the presence of residual motions. Only at $T = 80$ K the decay is a stretched exponential, typical of relaxation due to the interaction with surrounding paramagnetic centers, either nuclei or electrons, at low temperatures.[54]

The more suitable method to evidence the presence of residual intramolecular motions is the ED-EPR powder-like spectrum. In the presence of motions the ED-EPR spectrum shows an increasing distortion on increasing the inter-pulse delay τ with respect to the integrated CW-EPR profile. This is due to the dependence of the phase memory time T_M on the orientation of the principal axes of the anisotropic interactions with respect to the magnetic field. As can be obtained from eqn (1), the relaxation rate becomes faster on increasing the angle between the field and the principal axes.

We obtained satisfactory simulations of the ED-EPR spectra of NitSAc in the glassy matrix by taking into account a librational motion around an axis whose components in the $\boldsymbol{g}$ tensor eigenframe are approximately given by (0.10, 0.40, 0.91); assuming a correlation time equal to 30 ps,[42] the amplitude of the motion is restricted to a few degrees.

Above 120 K the echo decay becomes too fast with respect to the instrumental dead time; at the same temperature the CW-EPR spectrum shows slight modifications with respect to the 80 K spectrum, indicating the activation of a new motion. A candidate for this motion could be the intramolecular conformational interconversion of the five atom ring, discussed above.

Finally, when the phase memory time of NitSAc is compared with that of the CTPO at 80 K, where no specific intramolecular motions are active, the former is still longer by a factor of two, as T_M is equal to 2.8 μs for CTPO and to 5.4 μs for NitSAc.

These observations lead us to conclude that NitRs are promising candidates in view of potential applications, both in QIP and as spin probes. Indeed, one of the prerequisites for the use of these systems in quantum information applications is that the coherence times exceed by a large factor the time needed for coherent manipulations of electron spins, the ratio between the two being defined as the figure of merit for single-qubit operations.[14,18] With present technology the latter time scale is of the order of 10 ns for electron spins, thus leading, for NitSAc, to a figure of merit of about one hundred at room temperature and of several hundred at liquid nitrogen temperature. This is comparable to decoherence times reported for metal-based molecular magnets such as Cr_7Ni below liquid He temperature (T_M = 15.3 μs at 1.5 K)[23] and Fe_3 ($T_M = 2.6$ μs up to 7 K)[71] and much longer than those observed in an Fe_4 single molecule magnet ($T_M = 630$ ns at 4.3 K)[72] and in V_{15}, the first molecular magnet for which Rabi oscillations have been detected.[73,74]

As for their potential use as spin probes, the slower relaxation – especially of the transverse magnetization – makes possible the use of relatively long pulse experiments, as those used to measure distances between pairs of radicals (DEER[75–77]).

Conclusions

This study allowed the determination of the relaxation properties of a NitR molecule, NitSAc, which was explicitly designed to favor well-organized self-assembled monolayers.

For the first time the hyperfine interaction tensors for the ^{14}N nuclei of a NitR radical have been determined. The results show that the two nuclei have the same hyperfine isotropic coupling at high temperatures, but at low temperatures their pseudo-axial HF tensors are tilted by 9°. We conclude, also on the basis of the relaxation behaviour, that a fast interconversion motion of the five atoms ring in fluid solution averages the two ^{14}N hyperfine interactions, becomes slow in the soft glassy phase – preventing the detection of the echo in a restrict range of temperatures between 120 and 180 K – and brings to non-equivalent hyperfine tensors at lower temperatures.

The analysis of the relaxation data shows that both the T_1 and the T_2 (or T_M) relaxation times for NitSAc are longer by a factor of two than for a typical nitroxide (CTPO), both in fluid and in frozen toluene solution.

The detailed characterization of both static and dynamic paramagnetic properties of the former system, together with the availability of recent software for the interpretation of CW-EPR spectra,[78,79] paves the way toward the use of this and similar radicals as potential spin labels in advanced EPR applications. Further, the long T_2 (or T_M) and T_1 observed are particularly appealing in view of the use of this system as a potential qubit, with figure of merit larger than one hundred at both room and liquid nitrogen temperatures. In perspective it is then of much relevance to investigate whether these properties are maintained once the radical is organized in ordered addressable arrays of qubits obtained *e.g.* by exploiting the thioacetyl functions to promote self-assembling of monolayers.

Acknowledgements

This work is supported by Ministero dell'Istruzione, Università e Ricerca (MIUR), by grant 2008FZK5AC PRIN 2008. M. M., L. S. and D. G. acknowledge the financial support of EC through the FP7-People Marie Curie Action IAPP project 286196 and of MIUR through the PRIN *20097X44S7* "Record" Project.

References

1 J. H. Osiecki and E. F. Ullman, *J. Am. Chem. Soc.*, 1968, **90**, 1078–1079.
2 E. F. Ullman, J. H. Osiecki, D. G. B. Boocock and R. Darcy, *J. Am. Chem. Soc.*, 1972, **94**, 7049–7059.
3 A. Caneschi, D. Gatteschi, R. Sessoli and P. Rey, *Acc. Chem. Res.*, 1989, **22**, 392–398.
4 A. Caneschi, D. Gatteschi and P. Rey, in *Progress in Inorganic Chemistry*, John Wiley & Sons, Inc., New York, 1991, vol. 39, pp. 331–429.
5 M. Tamura, Y. Nakazawa, D. Shiomi, K. Nozawa, Y. Hosokoshi, M. Ishikawa, M. Takahashi and M. Kinoshita, *Chem. Phys. Lett.*, 1991, **186**, 401–404.
6 A. Caneschi, D. Gatteschi, N. Lalioti, C. Sangregorio, R. Sessoli, G. Venturi, A. Vindigni, A. Rettori, M. G. Pini and M. A. Novak, *Angew. Chem., Int. Ed.*, 2001, **40**, 1760–1763.
7 L. Bogani, C. Sangregorio, R. Sessoli and D. Gatteschi, *Angew. Chem., Int. Ed.*, 2005, **44**, 5817–5821.
8 K. Bernot, L. Bogani, A. Caneschi, D. Gatteschi and R. Sessoli, *J. Am. Chem. Soc.*, 2006, **128**, 7947–7956.
9 N. Ishii, Y. Okamura, S. Chiba, T. Nogami and T. Ishida, *J. Am. Chem. Soc.*, 2008, **130**, 24–25.
10 G. Poneti, K. Bernot, L. Bogani, A. Caneschi, R. Sessoli, W. Wernsdorfer and D. Gatteschi, *Chem. Commun.*, 2007, 1807–1809.
11 X.-L. Wang, L.-C. Li and D.-Z. Liao, *Inorg. Chem.*, 2010, **49**, 4735–4737.
12 H. Atsumi, K. Maekawa, S. Nakazawa, D. Shiomi, K. Sato, M. Kitagawa, T. Takui and K. Nakatani, *Chem.–Eur. J.*, 2012, **18**, 178–183.
13 K. Sato, S. Nakazawa, R. Rahimi, T. Ise, S. Nishida, T. Yoshino, N. Mori, K. Toyota, D. Shiomi, Y. Yakiyama, Y. Morita, M. Kitagawa, K. Nakasuji, M. Nakahara, H. Hara, P. Carl, P. Hofer and T. Takui, *J. Mater. Chem.*, 2009, **19**, 3739–3754.
14 M. Affronte, *J. Mater. Chem.*, 2009, **19**, 1731–1737.
15 A. Ardavan and S. J. Blundell, *J. Mater. Chem.*, 2009, **19**, 1754–1760.
16 J. Lehmann, A. Gaita-Arino, E. Coronado and D. Loss, *J. Mater. Chem.*, 2009, **19**, 1672–1677.
17 P. C. E. Stamp and A. Gaita-Arino, *J. Mater. Chem.*, 2009, **19**, 1718–1730.
18 F. Troiani and M. Affronte, *Chem. Soc. Rev.*, 2011, **40**, 3119–3129.
19 G. Aromí, D. Aguila, P. Gamez, F. Luis and O. Roubeau, *Chem. Soc. Rev.*, 2012, **41**, 537–546.
20 M. Mannini, L. Sorace, L. Gorini, F. M. Piras, A. Caneschi, A. Magnani, S. Menichetti and D. Gatteschi, *Langmuir*, 2007, **23**, 2389–2397.
21 P. Messina, M. Mannini, A. Caneschi, D. Gatteschi, L. Sorace, P. Sigalotti, C. Sandrin, S. Prato, P. Pittana and Y. Manassen, *J. Appl. Phys.*, 2007, **101**, 053916.
22 C. Simão, M. Mas-Torrent, N. Crivillers, V. Lloveras, J. M. Artés, P. Gorostiza, J. Veciana and C. Rovira, *Nat. Chem.*, 2011, **3**, 359–364.
23 C. J. Wedge, G. A. Timco, E. T. Spielberg, R. E. George, F. Tuna, S. Rigby, E. J. L. McInnes, R. E. P. Winpenny, S. J. Blundell and A. Ardavan, *Phys. Rev. Lett.*, 2012, **108**, 107204.
24 F. Meier, J. Levy and D. Loss, *Phys. Rev. B: Condens. Matter Mater. Phys.*, 2003, **68**, 134417.
25 A. Ardavan, O. Rival, J. J. L. Morton, S. J. Blundell, A. M. Tyryshkin, G. A. Timco and R. E. P. Winpenny, *Phys. Rev. Lett.*, 2007, **98**, 057201.
26 A. Schweiger and G. Jeschke, *Principles of Pulse Electron Paramagnetic Resonance*, Oxford University Press, Oxford, 2001.
27 V. Barone, M. Brustolon, P. Cimino, A. Polimeno, M. Zerbetto and A. Zoleo, *J. Am. Chem. Soc.*, 2006, **128**, 15865–15873.
28 A. Collauto, M. Zerbetto, M. Brustolon, A. Polimeno, A. Caneschi and D. Gatteschi, *Phys. Chem. Chem. Phys.*, 2012, **14**, 3200–3207.
29 V. Barone and A. Polimeno, *Phys. Chem. Chem. Phys.*, 2006, **8**, 4609–4629.
30 C.-J. Zhong and M. D. Porter, *J. Am. Chem. Soc.*, 1994, **116**, 11616–11617.
31 H. Takiguchi, K. Sato, T. Ishida, K. Abe, K. Yase and K. Tamada, *Langmuir*, 1999, **16**, 1703–1710.
32 G. Rajaraman, A. Caneschi, D. Gatteschi and F. Totti, *J. Mater. Chem.*, 2010, **20**, 10747–10754.
33 L. Poggini, Master thesis, University of Florence, 2011.
34 L. Gorini, PhD thesis, University of Florence, 2006.
35 L. Gorini, A. Caneschi and S. Menichetti, *Synlett*, 2006, 948–950.
36 M. J. Frisch, G. W. Trucks, H. B. Schlegel, G. E. Scuseria, M. A. Robb, J. R. Cheeseman, G. Scalmani, V. Barone, B. Mennucci, G. A. Petersson, H. Nakatsuji, M. Caricato, X. Li, H. P. Hratchian, A. F. Izmaylov, J. Bloino, G. Zheng, J. L. Sonnenberg, M. Hada, M. Ehara, K. Toyota, R. Fukuda, J. Hasegawa, M. Ishida, T. Nakajima, Y. Honda, O. Kitao, H. Nakai, T. Vreven, J. A. Montgomery, Jr, J. E. Peralta, F. Ogliaro, M. Bearpark, J. J. Heyd, E. Brothers, K. N. Kudin, V. N. Staroverov, T. Keith, R. Kobayashi, J. Normand, K. Raghavachari, A. Rendell, J. C. Burant, S. S. Iyengar, J. Tomasi, M. Cossi, N. Rega, J. M. Millam, M. Klene, J. E. Knox, J. B. Cross, V. Bakken, C. Adamo, J. Jaramillo, R. Gomperts, R. E. Stratmann, O. Yazyev, A. J. Austin, R. Cammi, C. Pomelli, J. W. Ochterski, R. L. Martin, K. Morokuma, V. G. Zakrzewski, G. A. Voth, P. Salvador, J. J. Dannenberg, S. Dapprich, A. D. Daniels, O. Farkas, J. B. Foresman, J. V. Ortiz, J. Cioslowski and D. J. Fox, *Gaussian 09, Revision B.01*, Gaussian, Inc., Wallingford, CT, 2010.
37 J. Tomasi, B. Mennucci and R. Cammi, *Chem. Rev.*, 2005, **105**, 2999–3094.
38 J. Cirujeda, J. Vidal-Gancedo, O. Jürgens, F. Mota, J. J. Novoa, C. Rovira and J. Veciana, *J. Am. Chem. Soc.*, 2000, **122**, 11393–11405.
39 S. Stoll and A. Schweiger, *J. Magn. Reson.*, 2006, **178**, 42–55.
40 E. Kirilina, S. Dzuba, A. Maryasov and Y. Tsvetkov, *Appl. Magn. Reson.*, 2001, **21**, 203–221.

41 A. Barbon, M. Bortolus, A. L. Maniero and M. Brustolon, *Phys. Chem. Chem. Phys.*, 2005, **7**, 2894–2899.
42 A. Barbon, M. Bortolus, M. Brustolon, A. Comotti, A. L. Maniero, U. Segre and P. Sozzani, *J. Phys. Chem. B*, 2003, **107**, 3325–3331.
43 J. A. Weil, *J. Magn. Reson.*, 1975, **18**, 113–116.
44 R. N. Schwartz, L. L. Jones and M. K. Bowman, *J. Phys. Chem.*, 1979, **83**, 3429–3434.
45 P. Höfer, Bruker Application Note no. 117.
46 E. A. Weiss, M. J. Tauber, M. A. Ratner and M. R. Wasielewski, *J. Am. Chem. Soc.*, 2005, **127**, 6052–6061.
47 M. Marrale, M. Brai, A. Barbon and M. Brustolon, *Radiat. Res.*, 2009, **171**, 349–359.
48 J. R. Harbridge, S. S. Eaton and G. R. Eaton, *J. Magn. Reson.*, 2002, **159**, 195–206.
49 D. E. Budil, K. A. Earle and J. H. Freed, *J. Phys. Chem.*, 1993, **97**, 1294–1303.
50 (*a*) T. Yoshino, S. Nishida, K. Sato, S. Nakazawa, R. D. Rahimi, K. Toyota, D. Shiomi, Y. Morita, M. Kitagawa and T. Takui, *J. Phys. Chem. Lett.*, 2011, **2**, 449–453; (*b*) S. Nakazawa, S. Nishida, T. Ise, T. Yoshino, N. Mori, R. D. Rahimi, K. Sato, Y. Morita, K. Toyota, D. Shiomi, M. Kitagawa, H. Hara, P. Carl, P. Höfer and T. Takui, *Angew. Chem., Int. Ed.*, 2012, DOI: 10.1002/anie.201204489.
51 J. A. D'Anna and J. H. Wharton, *J. Chem. Phys.*, 1970, **53**, 4047–4052.
52 V. I. Gulin, S. A. Dikanov, Y. D. Tsvetkov, I. A. Grigor'ev and I. A. Kirilyuk, *J. Struct. Chem.*, 1988, **29**, 472–475.
53 S. A. Dikanov, V. I. Gulin, Y. D. Tsvetkov and I. A. Grigor'ev, *J. Chem. Soc., Faraday Trans.*, 1990, **86**, 3201–3205.
54 A. Barbon, M. Brustolon, A. L. Maniero, M. Romanelli and L.-C. Brunel, *Phys. Chem. Chem. Phys.*, 1999, **1**, 4015–4023.
55 J. Goldman, T. E. Petersen, K. Torssell and J. Becher, *Tetrahedron*, 1973, **29**, 3833–3843.
56 T. Takui, Y. Miura, K. Inui, Y. Teki, M. Inoue and K. Itoh, *Mol. Cryst. Liq. Cryst. Sci. Technol., Sect. A*, 1995, **271**, 55–66.
57 A. Carrington, A. Hudson and G. R. Luckhurst, *Proc. R. Soc. London, Ser. A*, 1965, **284**, 582–593.
58 J. H. Freed and G. K. Fraenkel, *J. Chem. Phys.*, 1963, **39**, 326–348.
59 S. A. Goldman, G. V. Bruno, C. F. Polnaszek and J. H. Freed, *J. Chem. Phys.*, 1972, **56**, 716–735.
60 A. Collauto, A. Barbon and M. Brustolon, *J. Magn. Reson.*, 2012, **223**, 180–186.
61 P. J. W. Debye, *Polar Molecules*, Dover, New York, 1929.
62 J. H. Freed, *J. Chem. Phys.*, 1964, **41**, 2077–2083.
63 P. S. Hubbard, *Phys. Rev.*, 1963, **131**, 1155–1165.
64 P. W. Atkins and D. Kivelson, *J. Chem. Phys.*, 1966, **44**, 169–174.
65 A. Capiomont, B. Chion, J. Lajzerowicz-Bonneteau and H. Lemaire, *J. Chem. Phys.*, 1974, **60**, 2530–2535.
66 V. Barone, M. Zerbetto and A. Polimeno, *J. Comput. Chem.*, 2009, **30**, 2–13.
67 M. Brustolon and U. Segre, *Appl. Magn. Reson.*, 1994, **7**, 405–413.
68 J. R. Harbridge, S. S. Eaton and G. R. Eaton, *J. Phys. Chem. A*, 2003, **107**, 598–610.
69 H. Sato, S. E. Bottle, J. P. Blinco, A. S. Micallef, G. R. Eaton and S. S. Eaton, *J. Magn. Reson.*, 2008, **191**, 66–77.
70 N. P. Isaev, L. V. Kulik, I. A. Kirilyuk, V. A. Reznikov, I. A. Grigor'ev and S. A. Dzuba, *J. Non-Cryst. Solids*, 2010, **356**, 1037–1042.
71 G. Mitrikas, Y. Sanakis, C. P. Raptopoulou, G. Kordas and G. Papavassiliou, *Phys. Chem. Chem. Phys.*, 2008, **10**, 743–748.
72 C. Schlegel, J. van Slageren, M. Manoli, E. K. Brechin and M. Dressel, *Phys. Rev. Lett.*, 2008, **101**, 147203.
73 S. Bertaina, S. Gambarelli, T. Mitra, B. Tsukerblat, A. Muller and B. Barbara, *Nature*, 2008, **453**, 203–206.
74 J. Yang, Y. Wang, Z. Wang, X. Rong, C.-K. Duan, J.-H. Su and J. Du, *Phys. Rev. Lett.*, 2012, **108**, 230501.
75 M. Pannier, S. Veit, A. Godt, G. Jeschke and H. W. Spiess, *J. Magn. Reson.*, 2000, **142**, 331–340.
76 G. Jeschke and Y. Polyhach, *Phys. Chem. Chem. Phys.*, 2007, **9**, 1895–1910.
77 R. Dastvan, B. E. Bode, M. P. R. Karuppiah, A. Marko, S. Lyubenova, H. Schwalbe and T. F. Prisner, *J. Phys. Chem. B*, 2010, **114**, 13507–13516.
78 S. K. Misra, *J. Magn. Reson.*, 2007, **189**, 59–77.
79 M. Zerbetto, A. Polimeno and V. Barone, *Comput. Phys. Commun.*, 2009, **180**, 2680–2697.